Bioactive Materials 21 (2023) 20–31

Contents lists available at ScienceDirect

Bioactive Materials

journal homepage: www.keaipublishing.com/en/journals/bioactive-materials

Wet adhesive hydrogel cardiac patch loaded with anti-oxidative, autophagy-regulating molecule capsules and MSCs for restoring infarcted myocardium

Tengling Wu, Xiaoping Zhang, Yang Liu, Chunyan Cui, Yage Sun, Wenguang Liu *

School of Materials Science and Engineering, Tianjin Key Laboratory of Composite and Functional Materials, Tianjin University, Tianjin, 300350, China

ARTICLE INFO

Keywords:
Myocardial infarction
Sponge
Hydrogel patch
Wet adhesive
Autophagy

ABSTRACT

Hydrogel patch-based stem cell transplantation and microenvironment-regulating drug delivery strategy is promising for the treatment of myocardial infarction (MI). However, the low retention of cells and drugs limits their therapeutic efficacies. Here, we propose a prefixed sponge carpet strategy, that is, aldehyde-dextran sponge (ODS) loading anti-oxidative/autophagy-regulating molecular capsules of 2-hydroxy-β-cyclodextrin@resveratrol (HP-β-CD@Res) is first bonded to the rat's heart via capillary removal of interfacial water from the tissue surface, and the subsequent Schiff base reaction between the aldehyde groups on ODS and amino groups on myocardium tissue. Then, an aqueous biocompatible hydrazided hyaluronic acid (HHA) solution encapsulating mesenchymal stem cells (MSCs) is impregnated into the anchored carpet to form HHA@ODS@HP-β-CD@Res hydrogel in situ via click reaction, thus prolonging the in vivo retention time of therapeutic drug and cells. Importantly, the HHA added to outer surface consumes the remaining aldehydes to contribute to nonsticky top surface, avoiding adhesion to other tissues. The embedded HP-β-CD@Res molecular capsules with antioxidant and autophagy regulation bioactivities can considerably improve cardiac microenvironment, reduce cardiomyocyte apoptosis, and enhance the survival of transplanted MSCs, thereby promoting cardiac repair by facilitating angiogenesis and reducing cardiac fibrosis.

1. Introduction

Myocardial infarction (MI) caused by coronary artery blockage seriously threatens human health and life [1]. More than 25% of the myocyte population is destroyed within hours after MI [2]. The depletion of cardiomyocytes and the limited regeneration capacity of heart can reduce cardiac contraction, leading to adverse left ventricular remodeling and eventual heart failure [3–5]. Currently, the main treatment methods for MI include drug therapy and interventional surgery. Although these treatments can help delay the progression of disease, they fail to repair the infarcted myocardium [6–8].

Both animal models and clinical trials have shown that stem cell transplantation is a promising clinical treatment for MI, due to the secretion of various immunomodulatory cytokines beneficial for cardiac regeneration [9–11]. However, the harsh microenvironment, especially the excessive reactive oxygen species (ROS) generated in the infarcted heart, can not only cause the necrosis of native cardiomyocytes but also prevent the retention and survival of transplanted cells, which greatly reduces the therapeutic effect [12–14]. The excessive ROS can directly attack DNA, proteins, and cause cell necrosis. In turn, the excessive ROS-induced mitochondrial damage increases the production of ROS, forming a vicious circle [15]. Thus far, numerous ROS-scavenging biomaterials have been developed to reduce ROS level after MI through integrating ROS-scavenging agents [16–18] or loading antioxidants [12, 19]; however, less attention has been devoted to suppressing the production of ROS from its source.

Autophagy is a self-eating cycle mechanism for degrading misfolded proteins and damaged organelles, which is essential for maintaining cell homeostasis [20]. Studies have shown that autophagy aids in the recovery of cardiac function from prolonged ischemia after MI [21–23]. 2-hydroxypropyl-β-cyclodextrin (HP-β-CD) is well known as a complexing agent that can increase aqueous solubility and bioavailability of many therapeutic drugs [24]. In addition, recent studies have demonstrated that HP-β-CD can treat diseases (such as Parkinson's disease,

Peer review under responsibility of KeAi Communications Co., Ltd.
* Corresponding author.
E-mail address: wgliu@tju.edu.cn (W. Liu).

https://doi.org/10.1016/j.bioactmat.2022.07.029
Received 21 June 2022; Received in revised form 24 July 2022; Accepted 27 July 2022

Niemann-Pick disease, and atherosclerosis) by inducing an autophagic pathway [25–27]. However, the potential cardioprotection of HP-β-CD has not yet been reported so far.

Resveratrol (Res), a plant-produced polyphenol, has been shown to have cardioprotective effects due to its antioxidant and anti-inflammatory effects, by scavenging free radicals, inhibiting lipid peroxidation, and regulating the activity of enzymes-related antioxidation, but its poor water solubility limits its biofunction and in vivo application [28,29]. Herein, HP-β-CD was used to improve the water solubility of Res and molecular capsules (HP-β-CD@Res) were synthesized through host-guest interaction between HP-β-CD and Res. We supposed that HP-β-CD@Res integrated with antioxidant and autophagy bioactivities could significantly improve the adverse microenvironment and activate an autophagic pathway to reduce cardiomyocyte apoptosis after MI.

Considering the retention of transplanted cells and drugs in infarcted area, we engineered an adhesive hydrogel bearing HP-β-CD@Res and MSCs to efficiently improve cardiac function post-MI. Adhering hydrogels to heart surface is challenging, because the surficial water prevents direct contact of adhesive moieties with moist tissue [30]. Recently, encouraging progress in wet tissue adhesives has been made [31]. Nonetheless, achieving reliable adhesion of stem cells-loaded hydrogels without affecting cell viability remains elusive since the cells cannot survive in pre-dried gel or hostile treatment conditions required for realizing wet adhesion [32–34]. In this study, a wet tissue adhesive hydrogel (termed as HHA@ODS) was developed from aldehyde dextran sponge (ODS), into which HP-β-CD@Res molecular capsules were encapsulated. We hypothesized that the ODS@HP-β-CD@Res could rapidly bond to the wet soft tissue via the capillary removal of interfacial water from the tissue surface, and the subsequent occurrence of Schiff base reaction between the aldehyde groups on ODS and amino groups on myocardium tissue would lead to a firmly fixed sponge carpet. Then, an aqueous HHA solution mixed with MSCs was impregnated into the ODS@HP-β-CD@Res in situ to form HHA@ODS@HP-β-CD@Res hydrogel further by Schiff base reaction between the remaining aldehydes on the outmost ODS and hydrazides on the HHA, thereby fixing the MSCs loaded-HHA@ODS@HP-β-CD@Res hydrogel to the beating myocardial surface (Scheme 1). This would prolong the retention time of HP-β-CD@Res as well as MSCs on the infarcted myocardium. The embedded HP-β-CD@Res molecular capsules with antioxidant and autophagy regulation bioactivities would improve cardiac microenvironment, reduce cardiomyocyte apoptosis, and enhance the survival of transplanted stem cells, thus promoting cardiac repair by facilitating angiogenesis and reducing cardiac fibrosis. We hope this therapy strategy could address the intractable problems associated with MI treatment.

2. Materials and methods

2.1. Materials

Dextran (Dex, Mw = 200 kDa, Psaitong, China), hyaluronic acid sodium salt (HA, Mw = 50 kDa, Heowns, China), sodium periodate (99%, Sigma-Aldrich, USA), carbohydrazide (CDH, 97%, Heowns, China), resveratrol (Res, 98%, Heowns, China), 2-hydroxypropyl-β-cyclodextrin (HP-β-CD, 98%, Heowns, China), ethylene glycol (99%, Aladdin, China), 1-hydroxybenzotriazole (HOBT, 98%, Heowns, China), N-(3-dimethylaminopropyl)-N′-ethylcarbodiimide hydrochloride (EDC, aladdin, China), hydrogen peroxide (H_2O_2, 30 wt%, aladdin, China), 3-methyladenine (3-MA, 99%, MedChemExpress, USA), propidium iodide (PI, 99.44%, MedChemExpress, USA), Calcein acetoxymethyl ester (Calcein-AM, 95%, MedChemExpress, USA), 2′,7′-dichlorodihydrofluorescein diacetate (DCFH-DA, Solarbio, China), 5,5′,6,6′-tetrachloro-1,1′,3,3′-tetraethyl-imidacarbocyanine (JC-1, 99%, MedChemExpress, USA), mitochondrial superoxide indicator (MitoSOX Red, Yeasen, China), 1-diphenyl-2-picrylhydrazyl free radical (DPPH, 97%, TCI, China) and 3-(4,5-dimethyl-2-thiazoyl)-2,5-diphenyl tetrazolium bromide (MTT, 98%, Solarbio, China) were used as received. Antibodies of α-actinin, vWF and α-SMA were purchased from Santa Cruz Biotechnology (USA). The antibodies used in western blot were all obtained from Abcam (UK). All the other reagents were of analytical grade and used without further purification.

2.2. Synthesis of HP-β-CD@Res

0.308 g HP-β-CD was dissolved in 10 mL ethanol at room temperature. Then 0.0456 g Res dissolved in 2 mL ethanol was slowly dropwise to the above solution, and stirred for 4 h. The obtained solution was evaporated at room temperature to remove ethanol, and then the collected product was dissolved in deionized water, and the insoluble matter was removed with a 220 nm filter. The obtained filtrate was freeze-dried to obtain HP-β-CD@Res. The content of Res in HP-β-CD@Res was determined by UV–visible spectrophotometer (TU-1810 UV–vis spectrophotometer).

2.3. Synthesis of oxidized Dex (OD)

0.324 g Dex (Mw = 200 kDa) was dissolved in 50 mL deionized water at room temperature. Then a certain amount of sodium periodate was added to the solution, and reacted for 3 h. Subsequently, 10 mL ethylene glycol was added to the solution and kept stirring for 1 h to terminate the reaction. The obtained solution was dialyzed in deionized water for 3 days, and then OD was obtained after freeze-drying and stored at −20 °C for further use. The oxidation degree of OD was determined by

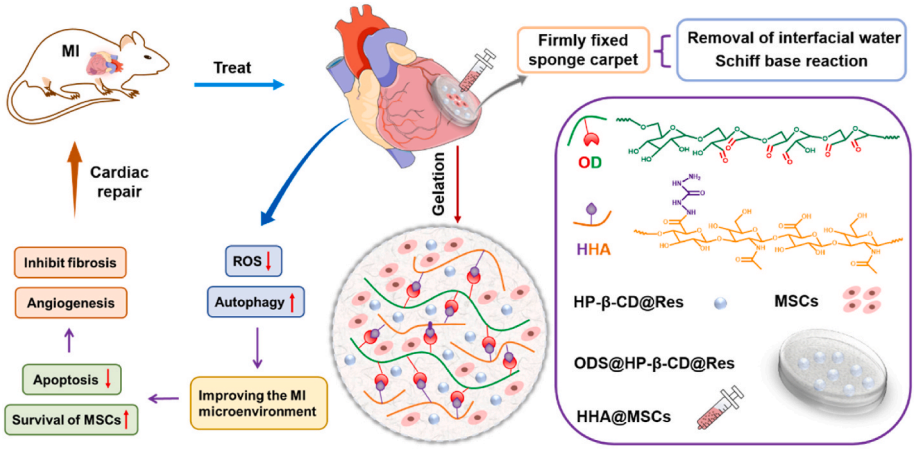

Scheme 1. Schematic illustration of the design of adhesive hydrogel system for the treatment of myocardial infarction.

measuring the aldehyde content using hydroxylamine hydrochloride titration method as previously reported [7].

2.4. Preparation of OD sponge (ODS)

OD was dissolved in deionized water and the concentration was fixed at 1 wt%. Then 250 μL OD solution was placed into 48 well plate and freeze-dried to obtain ODS.

2.5. Preparation of HHA@ODS hydrogels

The HHA@ODS hydrogels were synthesized by adding 50 μL HHA (2% m/v) solution onto ODS.

2.6. Measurement the adhesive strength of ODS

The adhesive strength of ODS was evaluated by lap-shear test on an electromechanical tester (WDW-05, Time Group Inc., China). The ODS with a diameter of 8 mm was sandwiched as an interlayer between two pieces of chicken myocardium tissue. The tensile rate was set at 5 mm/min and the maximal detachment stress of the sponge from the substrate was recorded as the adhesive strength.

2.7. Rheology test

The rheological properties of HHA@ODS hydrogels were tested on the Rheometer (MCR 302, Austria) configured with a 25 mm parallel plate. Time-sweep (0–10 min, 1 Hz, strain of 1%) and frequency-sweep (0.1–20 Hz, strain of 1%) results were both collected at 37 °C.

2.8. DCFH-DA fluorescence staining

DCFH-DA fluorescence staining was used to evaluate the intracellular ROS. 5×10^4 H9C2 cells were cultured in 24 well plate for 24 h. Then, the culture medium was replaced by fresh medium containing 700 μM H_2O_2 and drug, and further incubated for 5 h, and then the culture medium was discarded and the cells were treated by DCFH-DA for 10 min at 37 °C in dark. After being washed with HBSS, the cell morphology was observed under fluorescence microscope (Invitrogen EVOS M5000, USA).

2.9. Mitosox Red fluorescence staining

Mitosox Red fluorescence staining was used to evaluate the mitochondrial ROS. 5×10^4 H9C2 cells were cultured in 24 well plate for 24 h. Then, the culture medium was replaced by fresh medium containing 700 μM H_2O_2 and drug and further incubated for 5 h, and then the culture medium was discarded and the cells were treated by Mitosox Red for 10 min at 37 °C in dark. After being washed using HBSS, the cell morphology was observed under fluorescence microscope (Invitrogen EVOS M5000, USA).

2.10. JC-1 fluorescence staining

JC-1 staining was used to analyze mitochondrial membrane. 5×10^4 H9C2 cells were cultured in 24 well plate for 24 h. Then, the culture medium was replaced by fresh medium containing 700 μM H_2O_2 and drug and further incubated for 5 h, and then the culture medium was discarded and the cells were treated by JC-1 for 20 min at 37 °C in dark. After being washed using HBSS, the cell morphology was observed under fluorescence microscope (Invitrogen EVOS M5000, USA).

2.11. Western blot

The collected H9C2 cells were lysed with RIPA containing protease inhibitor. Total protein was separated by SDS-polyacrylamide gel electrophoresis (PAGE) and transferred onto polyvinylidene fluoride (PVDF) membranes (0.2 μm). The membrane was incubated with the anti-GAPDH (1:2000), anti-p62 (1:10000) and anti-LC3B (1:2000) antibodies at 4 °C overnight. After washing with TBST, the membranes were incubated with secondary antibodies for 4 h at room temperature. Subsequently, by further washing with TBST, the protein bands were imaged in a Gel Doc gel imaging system (Gel Doc XR+, Bio-Rad, USA) using Clarity™ Western ECL Substrate. The band intensity was quantified using Image J software.

2.12. Myocardial infarction model and treatment

MI animal model was established by ligating the left anterior descending of coronary artery according to the previous report [7]. Male SD rats (180-200 g) were randomly divided into MI, PBS, HP-β-CD, HP-β-CD@Res, HHA@ODS, HHA@ODS@MSCs, HHA@ODS@HP-β-CD@Res and HHA@ODS@HP-β-CD@Res@MSCs groups. Rats that received thoracotomy without ligating the left anterior descending were set as sham group. 100 μL PBS, HP-β-CD, HP-β-CD@Res solutions were respectively injected into the rats' myocardium. The implementation process of hydrogel patch: ODS was firstly applied to the surface of myocardial tissue, and then HHA solution was dropped onto ODS to form hydrogel on the surface of tissues. The chests of rats were immediately sutured after transplantation and receiving penicillin (intramuscular injection).

2.13. Echocardiographic assessment

The left ventricular (LV) functions of rats were evaluated by an echocardiography imaging system (Vevo 3100 Imaging System, VisualSonics, Canada) at 28 days after operation. Echocardiograms were collected and left ventricular ejection fraction (EF), left ventricular fractional shortening (FS) were analyzed to evaluate cardiac function.

2.14. Histological evaluation

On the 28th day after surgery, the cardiac tissues from different groups were harvested, and then the embedded heart sections were prepared. Masson trichrome staining was performed on these samples to analyze the cardiac structure. The cardiac images were collected by a fluorescence microscope (CKX41, Olympus, Japan) and the left-ventricular (LV) wall thickness and fibrosis area of the infarcted area were quantified by Image J software.

2.15. Immunofluorescence staining

The expression of DHE, Tunel, α-actinin, α-SMA and vWF of different groups were characterized by immunofluorescence staining. Briefly, cardiac tissue sections were incubated with primary antibody overnight at 4 °C, washed with PBS, and then incubated with secondary antibody. Then the samples were stained with DAPI. The images of sections were recorded with a Nikon inverted fluorescence microscope.

2.16. Statistical analysis

Data are presented as means ± standard deviations. Statistical significance was calculated by using Student's *t*-test for two-sample analyses and using one-way analysis of variance (ANOVA), followed by post hoc Bonferroni test for multiple sample analyses. Statistical differences were defined as $^*p < 0.05$, $^{**}p < 0.01$.

3. Results and discussion

3.1. Preparation and characterization of HP-β-CD@Res

HP-β-CD@Res was synthesized through the host-guest interaction

between HP-β-CD and Res in alcohol solution (Fig. 1A). FTIR and XRD were used to characterize the synthesis of HP-β-CD@Res inclusion complexes. As shown in Fig. 1B, the characteristic peaks of Res were observed at 1606, 1587, 1384, and 965 cm^{-1}, which corresponded to the C–C aromatic double bond stretching, C–C olefinic, C–O stretching and trans olefinic bond, respectively. The feature peak at 3407 cm^{-1} was assigned to the vibration of the hydrogen bonded OH groups of HP-β-CD, and some other intense peaks at 1654, 1156, and 1032 cm^{-1} were respectively ascribed to the H–O–H bending, C–O and C–O–C stretching [35]. In the spectra of the two solid physical mixtures (HP-β-CD+Res), all characteristic bands of Res and HP-β-CD were clearly observed, suggesting weaker or no interaction between Res and HP-β-CD in a solid physical mixture. In comparison, in the spectra of HP-β-CD@Res, some characteristic bands of Res are absent, suggesting the formation of the HP-β-CD@Res inclusion complexes [36]. In the XRD patterns (Fig. 1C), pure Res was highly crystallized and exhibited strong crystalline peaks in the range of 5°–50°. The XRD pattern of HP-β-CD displayed a broad peak, implying an amorphous structure. Clearly, the HP-β-CD+Res solid physical mixture exhibited corresponding characteristic peaks of Res and HP-β-CD, while the diffraction peaks of Res were invisible in the HP-β-CD@Res, further confirming the formation of inclusion complex [35]. The interaction of host-guest complexes was also characterized by ^{1}H NMR spectroscopy. As shown in Fig. 1E and F, the chemical shift (δ) of Res wrapped by HP-β-CD moved to the higher field due to the host-guest interaction of HP-β-CD and Res. And the protons inside the HP-β-CD cavity showed the maximum chemical shift change, △δ, which was consistent with the previous report [35].

The content of Res in HP-β-CD@Res was determined to be about 9.8 wt% by ultraviolet–visible spectroscopy (UV–Vis). Then, the ROS scavenging activity of HP-β-CD@Res was evaluated by diphenyl-2-picrylhydrazyl free radical (DPPH) and hydroxyl radicals (OH·) scavenging experiment. Fig. 1F exhibits that the DPPH solution treated with Res and HP-β-CD@Res changed from purple to yellow, whereas the HP-β-CD treatment caused no change of the color, which was close to the control group, implying that Res and HP-β-CD@Res could effectively remove the DPPH radicals while HP-β-CD had no anti-oxidant activity. Subsequently, phenanthroline-Fe^{2+} oxidation method was used to test the OH· scavenging ability of HP-β-CD@Res. Phenanthrene-Fe^{2+} aqueous solution could be oxidized to phenanthrene-Fe^{3+} by OH· so that the maximum absorption peak of phenanthrene-Fe^{2+} at 536 nm disappeared (or decreased) [37], which was reflected in the lightening of the color of solution. As illustrated at Fig. 1G, the phenanthrene-Fe^{2+} solution treated with Res or HP-β-CD@Res could inhibit evidently the lightening of phenanthrene-Fe^{2+} solution colors while HP-β-CD could not, implying that Res and HP-β-CD@Res could scavenge OH·. The scavenging effect of Res and HP-β-CD@Res on DPPH free radicals and OH· could reach more than 60% determined by UV–Vis, whereas HP-β-CD barely had the ROS scavenging activity, further indicating that the ability of HP-β-CD@Res to scavenge ROS came from Res (Fig. 1I).

3.2. Attenuation of oxidative stress damage through antioxidant and upregulating autophagy pathway

Numerous ROS species generated in the infarcted myocardium after MI can cause oxidative stress damage in host cells. Before exploring the protective effect of HP-β-CD@Res on cardiomyocytes under oxidative

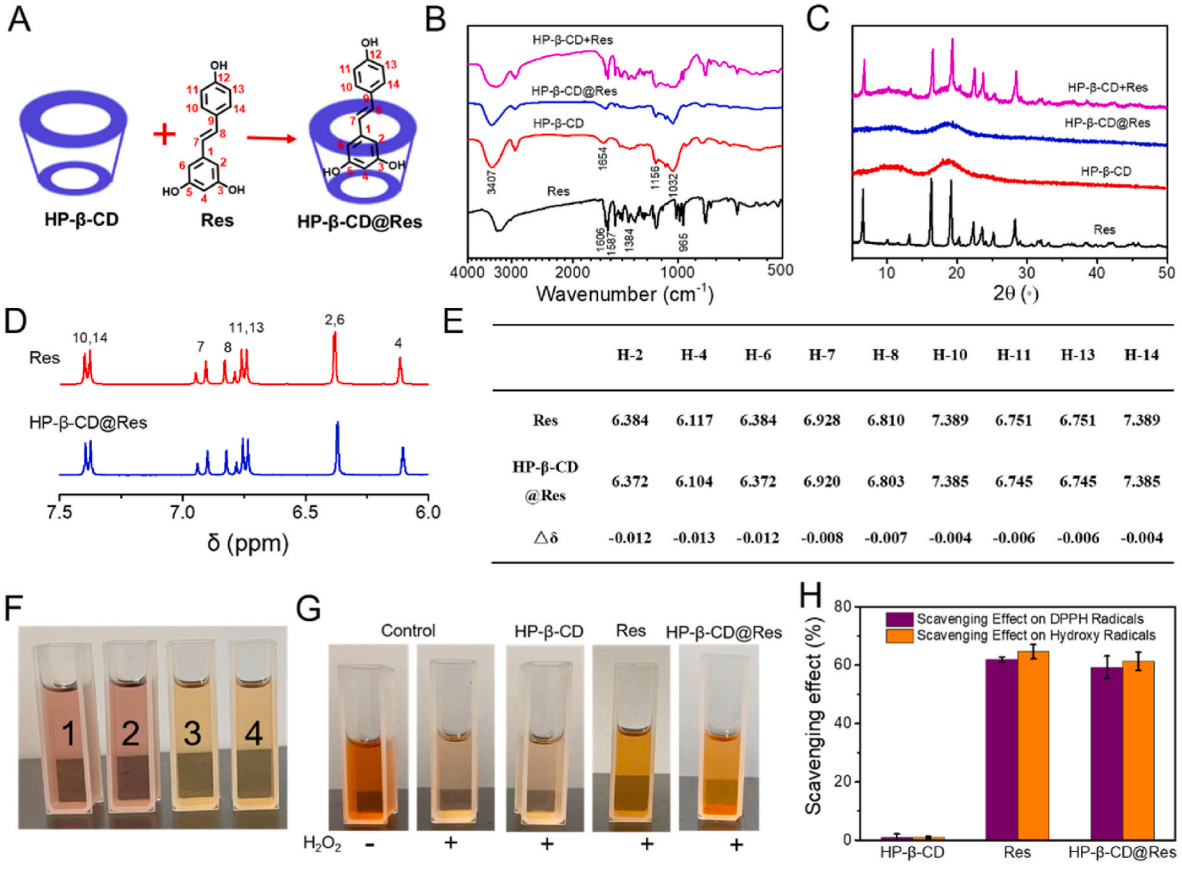

Fig. 1. Characterization of HP-β-CD@Res and its capacity to scavenge free radicals. (A) Preparation of HP-β-CD@Res. (B) FTIR spectra of Res, HP-β-CD, HP-β-CD@Res and HP-β-CD+Res. (C) XRD spectra of Res, HP-β-CD, HP-β-CD@Res and HP-β-CD+Res. (D) ^{1}H NMR spectra (expanded between 7.5 and 6.0 ppm) of Res and HP-β-CD@Res. (E) Comparison of the δ value for various protons of Res and HP-β-CD@Res. (F) Photographs of DPPH solutions with different treatments (1: Control; 2: HP-β-CD; 3: Res; 4: HP-β-CD@Res). (G) Photographs of phenanthrene-Fe^{2+} aqueous solutions with different treatments. (H) Scavenging effect of HP-β-CD@Res on DPPH radicals and OH· radicals.

stress, the optimal concentration of HP-β-CD@Res was first screened. The cytotoxicity of HP-β-CD and HP-β-CD@Res with various concentrations was determined by MTT assay. It is seen that the HP-β-CD did not cause significant cytotoxicity against normal H9C2 cardiomyocytes even at a concentration up to 0.9 mM (Fig. S1). And when the content of Res in HP-β-CD@Res reached 60 μM and the corresponding HP-β-CD concentration was 90 μM, almost no toxicity was detected against normal H9C2 cardiomyocytes (Fig. S2). In the following experiment, we determined the protective effects of HP-β-CD and HP-β-CD@Res on H_2O_2-treated H9C2 cardiomyocytes. As illustrated in Fig. S3, the HP-β-CD could reduce H_2O_2-induced cardiomyocytes death. Especially when the concentration of HP-β-CD was 90 μM, the viability of cardiomyocytes could maintain 80% while the viability of unprotected cardiomyocytes was only 66% under oxidative stress conditions. These results indicate that HP-β-CD could protect H9C2 cardiomyocytes against H_2O_2-induced injury by other mechanisms rather than through OH· scavenging pathway. In addition, when the concentration of Res in HP-β-CD@Res was 6 μM and the corresponding HP-β-CD concentration was 9 μM, the survival rate of cardiomyocytes could be rescued to 83% (Fig. S4), which was higher than that of the cardiomyocytes treated with 9 μM HP-β-CD, further indicating that HP-β-CD and Res could synergistically reduce H_2O_2-induced oxidative stress injury. Considering that 90 μM of HP-β-CD exhibited a better protective effect on cardiomyocytes than 9 μM, HP-β-CD@Res containing 6 μM Res was combined with 81 μM HP-β-CD (final concentration of HP-β-CD is 90 μM) and its protective effect on cardiomyocytes was determined. As expected, the survival rate of cardiomyocytes was further improved and reached as high as 90% (Fig. S5). Therefore, HP-β-CD (90 μM) and HP-β-CD@Res (90 μM HP-β-CD+6 μM Res) were used to conduct the next experiments. As mentioned above, HP-β-CD had no OH·-scavenging activity, so we speculate that the protective effect of HP-β-CD on cardiomyocytes came from its promotion of autophagy in cardiomyocytes. Western blot was employed to detect the expression levels of autophagy associated proteins LC3 II and p62. The autophagy substrates LC3-II and p62 were both degraded with the autophagic cargo in the autolysosome, and the accumulation of LC3-II and p62 aggregates is regarded as a robust marker of impaired autophagic flux [38]. Fig. 2A and B demonstrate that HP-β-CD and HP-β-CD@Res could enhance the expression of LC3 II but reduce the accumulation of p62 protein, indicating that autophagy flux has not been destroyed. This indicates that HP-β-CD and HP-β-CD@Res could enhance autophagy in cardiomyocytes. Previous studies have shown that HP-β-CD could activate transcription factor EB (TFEB), a master regulator of the autophagy-lysosomal pathway, to promote autophagy [26], and Res could enhance the formation of autophagosome [39]; thus, we speculate that HP-β-CD@Res could enhance autophagy by promoting the biogenesis of autophagosomes. To further demonstrate that HP-β-CD and HP-β-CD@Res-induced reduced oxidative stress injury was originated from the improvement of autophagy in cardiomyocytes, 3-methyladenine (3-MA), an autophagy antagonist, was introduced to the following experiments. As shown in Fig. S6, in the

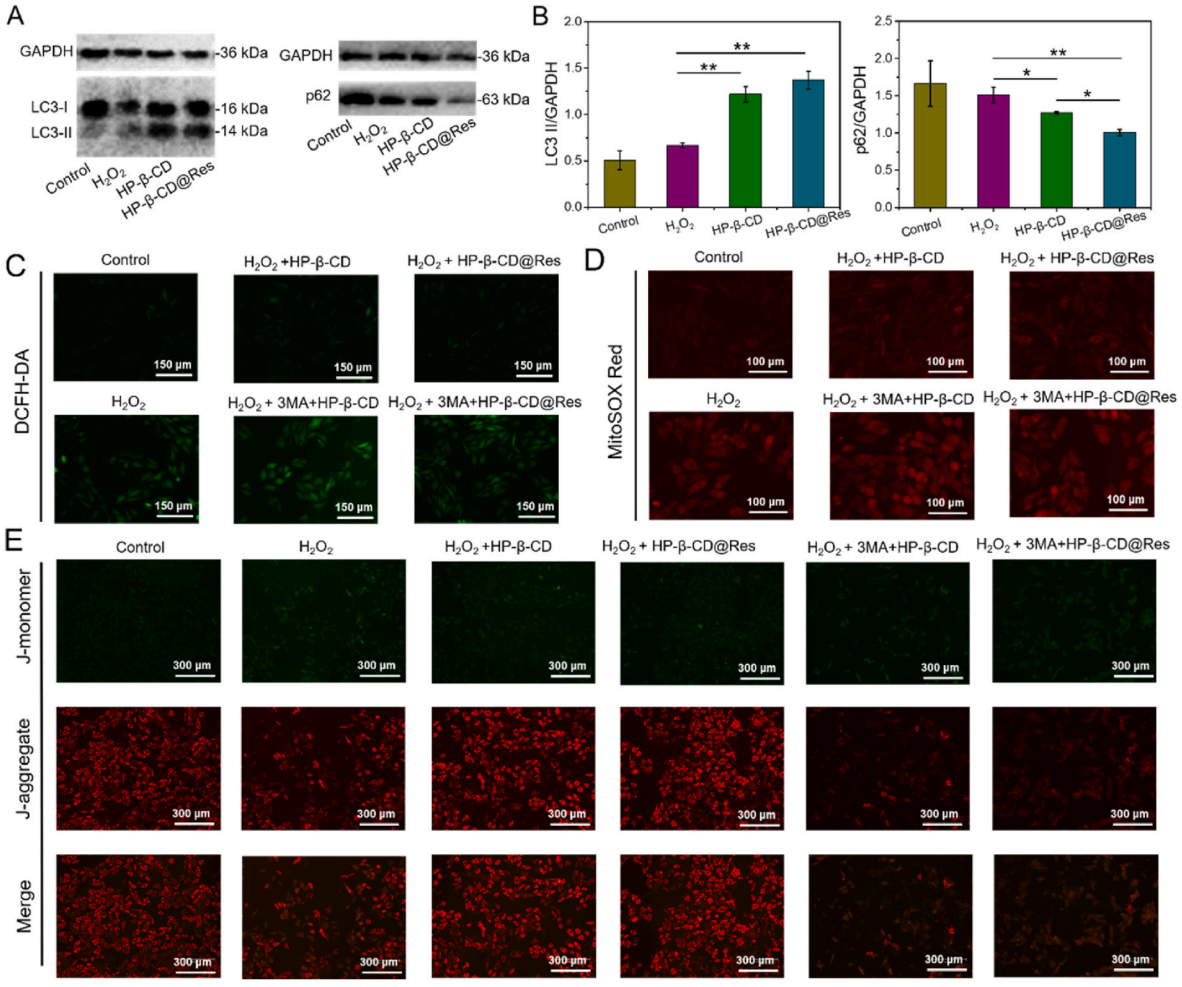

Fig. 2. Effects of HP-β-CD@Res on the expression of autophagy related protein, intracellular ROS, mitochondrial ROS and mitochondrial function in H9C2 cardiomyocytes. (A) Expression levels of LC3-I, LC3-II and p62 in control group, H_2O_2 group, H_2O_2+HP-β-CD group and H_2O_2+HP-β-CD@Res group were evaluated by western blot and (B) quantified by Image J software. (C) Representative images of intracellular ROS (DCFH-DA, green) of different groups. (D) Representative images of mitochondria ROS (MitoSOX Red, red) of different groups. (E) Representative JC-1 images of different groups.

presence of 3-MA, HP-β-CD and HP-β-CD@Res failed to reduce the oxidative stress damage in cardiomyocytes. It should be noted that although the ROS scavenging effect of Res could also protect cells against oxidative stress damage, 3-MA inhibited the autophagy of cardiomyocytes, so the cells were in poor condition, showing low viability. These data indicated that HP-β-CD and HP-β-CD@Res induced-autophagy was essential in the process of protection of cardiomyocytes.

In addition, 2′,7′-dichlorofluorescin diacetate (DCFH-DA) was used to evaluate the intracellular ROS level. Fig. 2C exhibits that strong green fluorescence (DCFH-DA) could be observed in H_2O_2 group indicating that the level of intracellular ROS increased significantly when treated with H_2O_2. However, when the cells were treated with HP-β-CD or HP-β-CD@Res, the intracellular ROS level decreased considerably, indicating that exogenous HP-β-CD or HP-β-CD@Res could reduce the ROS level. One of the functions of autophagy is to maintain the normal mitochondrial membrane potential and reduce the production of new ROS [4]. Therefore, we set to detect the levels of mitochondrial ROS and mitochondrial membrane potential by mitochondrial superoxide indicator (MitoSOX Red) and 5,5′,6,6′-tetrachloro-1,1′,3,3′-tetraethyl-imidacarbocyanine (JC-1) staining, respectively. As illustrated in Fig. 2D, the level of mitochondrial ROS was also reduced after treated with HP-β-CD or HP-β-CD@Res. Additionally, the mitochondrial membrane potential was shown to decrease (red fluorescence decreased) in the H_2O_2 group. After HP-β-CD treatment, the decline of mitochondrial membrane potential was mitigated; while HP-β-CD@Res treatment led to a further attenuation in the decrease of mitochondrial membrane potential (Fig. 2E). These indicated that HP-β-CD and HP-β-CD@Res could restore mitochondrial function. Previous studies have demonstrated that mitochondria are the main organelles for ROS production [40]; thus, introduction of HP-β-CD or HP-β-CD@Res could suppress the generation of ROS from its principal source. The inhibitive effect of 3-MA on the protective role of HP-β-CD or HP-β-CD@Res suggested that autophagy was involved in the protective effect of HP-β-CD or HP-β-CD@Res, which aided in reducing oxidative stress damage in cardiomyocytes and restoring mitochondrial function.

3.3. *Angiogenic capacities of HP-β-CD@Res and restoration of cardiac function*

Previous studies have shown that HP-β-CD could significantly increase angiogenesis [41], so we next examined the impact of HP-β-CD

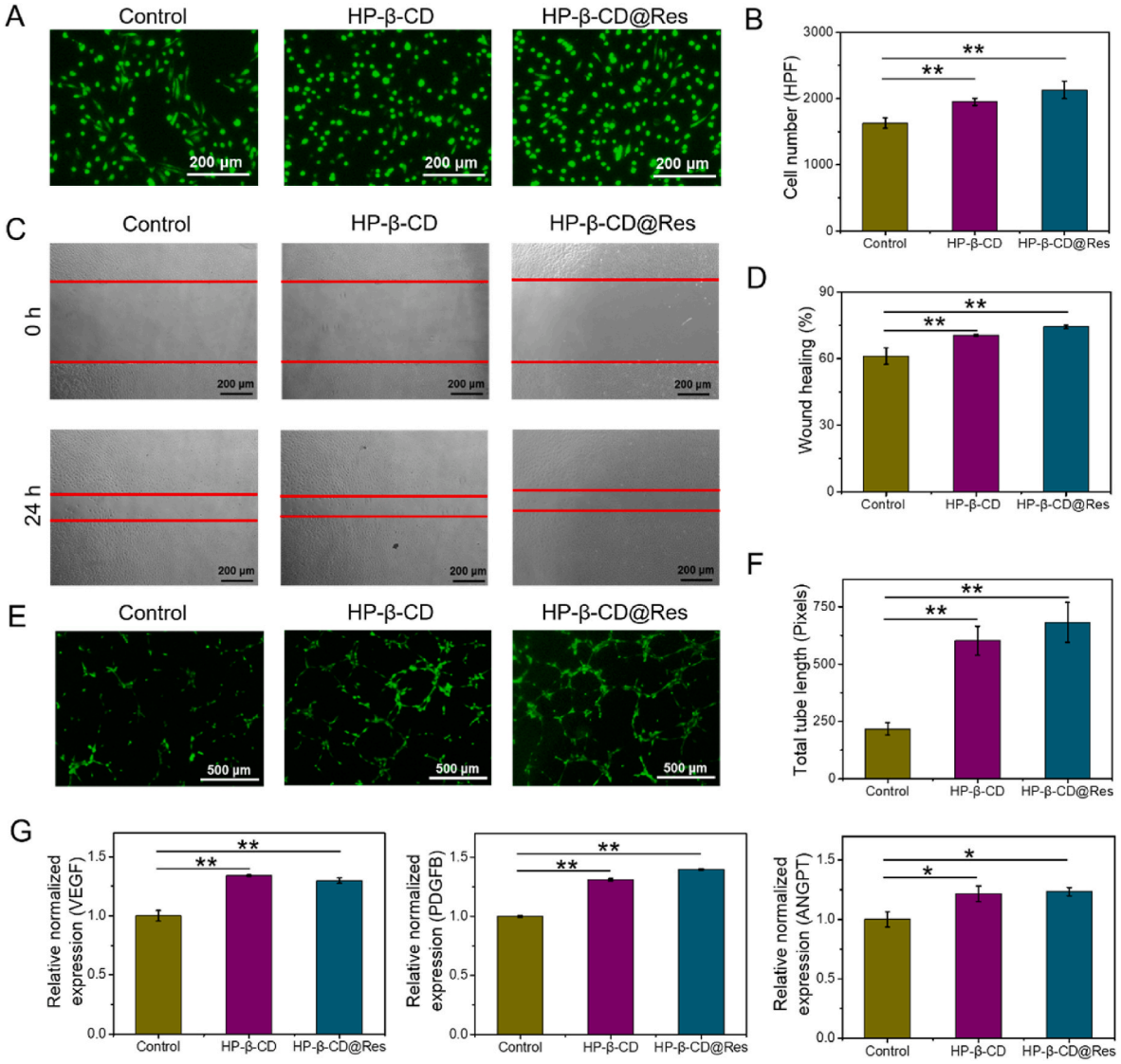

Fig. 3. HP-β-CD@Res-activated angiogenic capacities of HUVECs in vitro. (A) Proliferation was detected by AM staining and (B) quantified by the cell numbers. (C) Cell migration was assessed by wound-healing assay. (D) Quantitative analysis of wound-healing assay. (E) Tube formation capacity on the Matrigel and (F) analyzed by Image J software. (G) mRNA expression levels of VEGF, PDGFB and ANGPT evaluated by RT-PCR.

and HP-β-CD@Res on functions of human umbilical vein endothelial cells (HUVECs). HUVECs proliferation was assessed by Calcein-AM, and the results showed that HP-β-CD and HP-β-CD@Res could effectively promote the proliferation of HUVECs (Fig. 3A and B). Then, the effects of HP-β-CD and HP-β-CD@Res on the angiogenic capacity of HUVECs were evaluated by migration and tube formation assays. The results demonstrated that HP-β-CD and HP-β-CD@Res could promote the migration (Fig. 3C and D) and tube formation (Fig. 3E and F) of HUVECs. The quantitative real-time PCR (RT-PCR) results showed that pro-angiogenic genes (VEGF, PDGFB, ANGPT) were significantly upregulated after treatment with HP-β-CD and HP-β-CD@Res (Fig. 3G), manifesting that HP-β-CD and HP-β-CD@Res could activate the

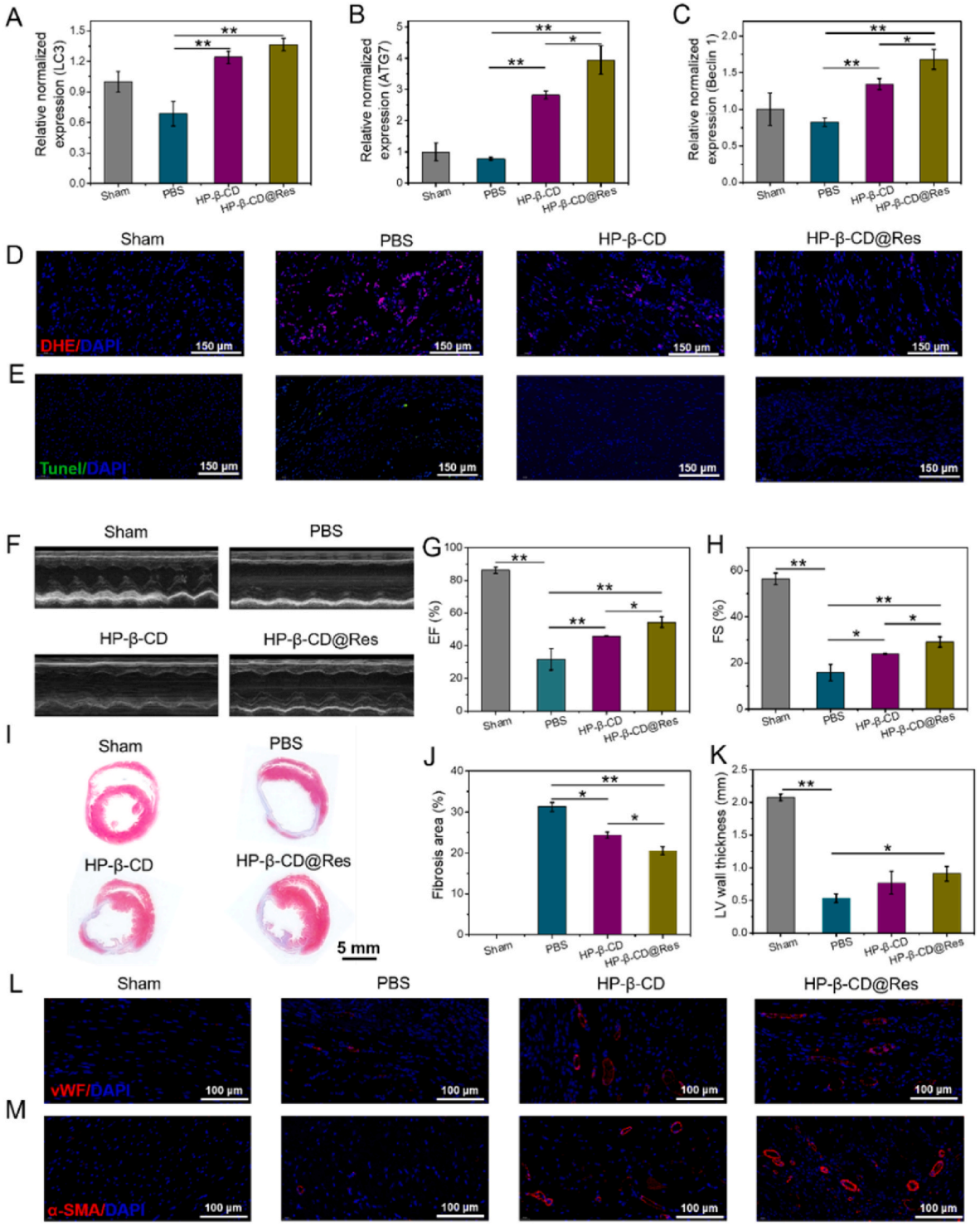

Fig. 4. Repair effect of different groups in MI rats. (A) mRNA expression levels of LC3, (B) ATG7 and (C) Beclin1 were evaluated by RT-PCR. (D) Representative immunofluorescent staining images of DHE. (E) Representative immunofluorescent staining images of Tunel positive cells at the infarcted area in various groups. (F) Left-ventricular function determined with echocardiography 28 days after the transplantation in different groups. (G) Quantification analysis of cardiac function of EF and (H) FS. (I) Cardiac structures as indicated by the Masson trichrome staining. (J) Quantitative analysis of the fibrosis area and (K) LV wall thickness. (L) Representative immunofluorescent staining images of vWF and (M) α-SMA.

angiogenic capacity of HUVECs.

To examine the effect of HP-β-CD and HP-β-CD@Res on the improvement of microenvironment in vivo, gene expression analyses and DHE immunofluorescence staining were performed with rat's heart tissues harvested 2 days after HP-β-CD and HP-β-CD@Res injection into infarcted myocardium. RT-PCR results showed that HP-β-CD and HP-β-CD@Res significantly upregulated the expression of several autophagy-related genes, such as LC3, ATG7 and Beclin1 in comparison with the PBS control hearts (Fig. 4A–C). DHE immunofluorescence staining was then used to determine the intracellular superoxide anions level. As illustrated in Fig. 4D, the expression of DHE fluorescence was considerably increased in infarcted tissues of PBS group compared with Sham group, indicating that a large amount of ROS accumulated in the infarcted myocardium after MI. While treatment of HP-β-CD or HP-β-CD@Res could effectively suppress the generation of intracellular ROS. We then measured the expressions of oxidative stress-related genes of NAD(P)H quinone dehydrogenase 1 (NQO1) and NADPH oxidase 4 (NOX4) by using the rat cardiac tissues harvested at 2 days post-implantation (Fig. S7). NQO1 is an enzyme responsible for cellular defense against oxidative damage, whereas NOX4 is upregulated during oxidative injury and inflammation. The HP-β-CD and HP-β-CD@Res groups were shown to significantly enhance the expression of NQO1 gene and downregulate the expression of NOX4 gene compared to PBS group, hinting that the improvement of ROS microenvironment in MI hearts. It was noted that HP-β-CD@Res exhibited a better effect, which was consistent with the in vitro results. Then, terminal deoxynucleotidyl transferase-mediated deoxyuridine triphosphate nick end labeling (Tunel) assay was used to evaluate the apoptosis of cardiomyocytes. Fig. 4E exhibits that HP-β-CD and HP-β-CD@Res could considerably alleviate apoptosis of cardiomyocytes compared with PBS group.

Echocardiography was then used to assay the cardiac function of SD rats at 28 days post-operation (Fig. 4F). As shown in Fig. 4G and H, the ejection fraction (EF) and fractional shortening (FS) of PBS group decreased significantly compared to Sham group indicating significant deterioration and severe infarction enlargement of heart after MI. After treated with HP-β-CD and HP-β-CD@Res, both EF (HP-β-CD: 45.94% ± 0.31%, HP-β-CD@Res: 54.42% ± 3.19% vs PBS: 31.70% ± 6.59%) and FS (HP-β-CD: 23.87% ± 0.29%, HP-β-CD@Res: 29.12% ± 2.27% vs PBS: 15.83% ± 3.56%) were improved compared with the PBS group. However, the cardiac function was still far from restoring the level of the Sham group (EF: 86.16% ± 1.84%, FS: 56.42% ± 2.48%). Masson trichrome staining was also used to observe the fibrosis size and LV wall thickness of the myocardium, and Image J software was employed to quantify fibrosis area and LV wall thickness. All infarcted areas were shown to exhibit fibrotic tissues, thinning of ventricular wall and ventricular dilation to different degrees (Fig. 4I–K). PBS-treated MI rats underwent the most severe infarction with the highest fibrosis area and the thinnest LV wall thickness compared with the HP-β-CD and HP-β-CD@Res groups. Comparatively, the HP-β-CD@Res group achieved the most significant inhibitory effect on fibrosis and LV dilation.

The revascularization of the infarcted area after MI plays an important role in cardiac repair. In in vitro experiments we have confirmed that HP-β-CD and HP-β-CD@Res could promote angiogenesis. Next, the angiogenesis in the infarct area of myocardial tissues was assayed by immunofluorescence analysis. Antibodies against vWF and α-SMA were used to determine the generation of microvascular density and small arterioles in the infarcted area. As shown in Fig. 4L–M, there was no neovascularization in the Sham group because angiogenesis hardly occurred in the normal myocardium [42]. Only a small amount of angiogenesis was found in the PBS group, while the formation of new blood vessels in the infarcted area was significantly promoted after treated with HP-β-CD or HP-β-CD@Res. The HP-β-CD@Res group resulted in the highest angiogenesis activity, which was beneficial to the revascularization of the infarcted area (Fig. S8). Based on these results, HP-β-CD@Res demonstrated the best therapeutic effect on the cardiac repair after MI. However, its improvement of cardiac function and cardiac structure was far from meeting the clinical needs due to the rapid clean-up of HP-β-CD and HP-β-CD@Res from the body.

3.4. Preparation and characterization of ODS/HHA hydrogels

Recently, the adhesive hydrogel cardiac patches have received increasing attention, because their mechanical support can reduce ventricular wall stress, decrease the LV cavity size, and restore the LV shape [43]. In addition, they can not only avoid injury from intramyocardial injection but also enable local and sustainable release of drugs, bioactive factors and cells. However, developing adhesive stem cells-loaded hydrogel patch with instantly robust adhesive strength in bonding wet tissue is challenging since adhesion condition is normally not conductive to cell survival. Herein, the HP-β-CD@Res was first encapsulated into the aldehyde dextran sponge (ODS), and bonded to the surface of wet myocardium as a fixed carpet. Then, an aqueous biocompatible HHA solution loading MSCs was impregnated into the fixed carpet to form HHA@ODS@HP-β-CD@Res hydrogel in situ via Schiff base reaction, thereby prolonging the retention time of HP-β-CD@Res as well as MSCs.

To make this adhesive hydrogel patch, we set out to prepare three aldehyde dextrans (ODs) with different oxidation degrees. Hydroxylamine hydrochloride method was used to determine the oxidation degrees of the three ODs, which were 60.1%, 33.2% and 15.8% and defined as OD-H, OD-M and OD-L, respectively. As shown in Fig. S9, a new peak at 1730 cm^{-1} appeared in the FTIR spectrum of OD compared with pristine dextran (Dex), which was attributed to the C═O stretching vibration of –CHO [44], confirming the successful synthesis of OD. In this experiment, HHA with 55% substitution degree of hydrazide group was used according to our previous report [45]. ODS was prepared by dissolving OD with 1% solid content in water, and then placing 250 μL of the solution in a 48-well plate, and freeze-drying. The diameter and thickness of the resultant ODS were approximately 8 mm and 2 mm, respectively. Next, we measured the adhesion of ODS and Dex sponge to myocardial tissue. We can find that ODS could bond two pieces of myocardium tissue together, but Dex sponge could not (Videos S1 and S2), suggesting that Schiff base bonds formed by the aldehyde groups of ODS and the amino groups on the tissue contributed to robust adhesion. The wet adhesive strength of ODS to myocardial tissue measured by lap-shear test was enhanced from 21 kPa to 33 kPa with an increase of the oxidation degree (Fig. 5A and B). With increasing oxidation degree, more aldehyde groups reacted with amino groups on myocardial tissues, thus leading to increased interfacial bonding strength. Considering that too many aldehyde groups may cause cytotoxicity, ODS-L with a lower degree of substitution was used in the following experiments and defined as ODS. As shown in Fig. S10, the ODS could not scavenge DPPH radicals and OH·. Then, the stability of ODS in PBS was measured. As shown in Fig. S11, the ODS could remain in PBS for a certain period (Video S3); however, it was dissolved completely after 1 h, which was not suitable for long-term use as cardiac patch. Therefore, HHA was introduced into the hydrogel patch. The hydrazide groups on HHA could rapidly cross-link with the aldehyde groups on ODS to form hydrogels through click reaction. This could not only enhance the stability of cardiac patch (remained stable in PBS, Fig. S10 and Video S4), but also improve cytocompatibility (the cell viability of ODS was only 63% but HHA-2%@ODS could be maintained above 95%) (Fig. S12) due to consumption of aldehyde. Scanning electron microscopy (SEM) image revealed that ODS had large pores, which was conducive to the absorption of surficial liquid to realize tissue adhesion. After crosslinking with HHA, the thickness of HHA@ODS hydrogel declined to 0.4 mm and the pore size became much smaller, which was favorable for entrapment of stem cells. The rheological and viscoelastic properties of the HHA@ODS hydrogel showed that in both time-sweep model and frequency-sweep mode, the storage modulus (G′) was always higher than the loss modulus (G″), indicating that hydrogel exhibited a solid-like behavior and viscoelasticity. The stability of the hydrogel was

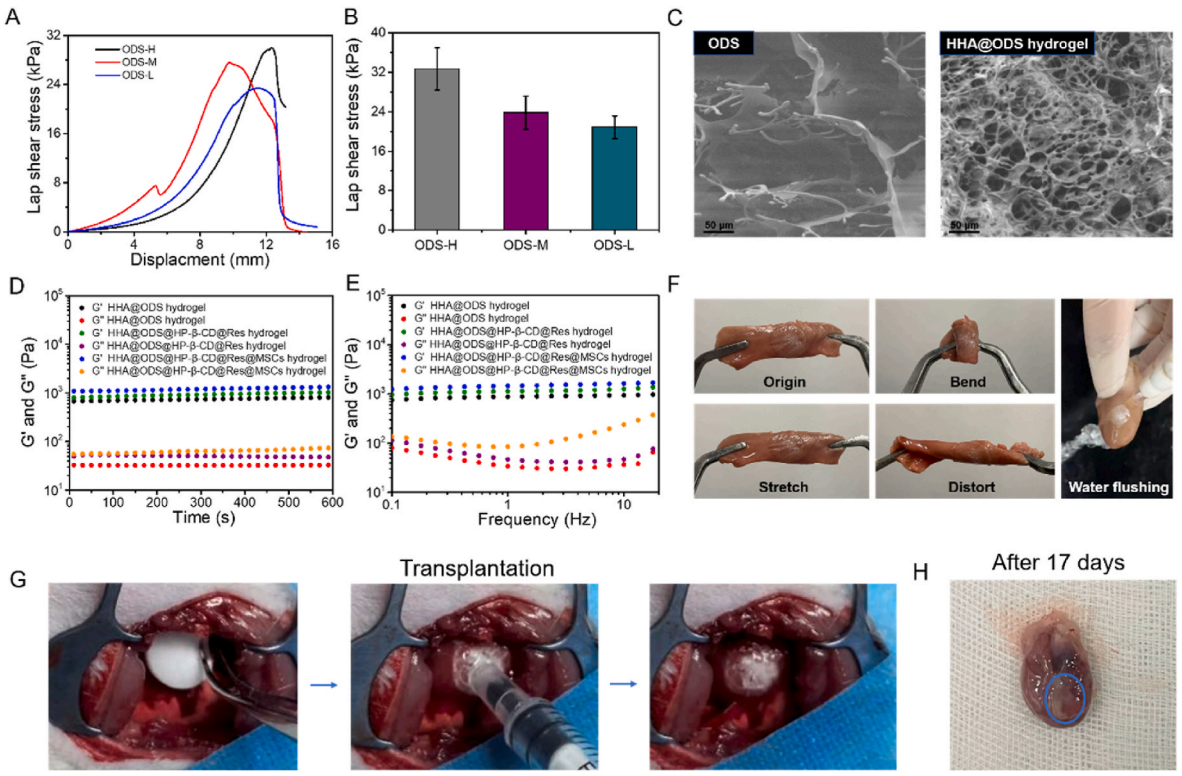

Fig. 5. Evaluation of the adhesive strength, morphological and rheological characteristics of ODS and HHA@ODS hydrogels. (A) Adhesion mechanical curves of ODS with varied oxidation degree to the chicken myocardium tissue. (B) Average adhesive strength of ODS with varied oxidation degree to the chicken myocardium tissue. (C) SEM images of ODS and HHA@ODS hydrogel. (D) Rheological analysis of hydrogels in a time-sweep mode at 37 °C. (E) Frequency-sweep tests of the hydrogels at 37 °C. (F) Photographs of the HHA@ODS hydrogel formed in situ on the chicken myocardium tissue. Bending, stretching, distorting, and water-flushing caused no detachment of the sample. (G) Transplantation process of HHA@ODS hydrogel to cardiac tissue in vivo. (H) Photograph of the HHA@ODS hydrogel after 17 days of transplantation into the myocardium.

not affected after loading the HP-β-CD@Res and MSCs (Fig. 5D and E). The adhesion of HHA@ODS hydrogel to myocardial tissues was measured in vitro and in vivo. As shown in Fig. 5F, ODS was firstly applied to the surface of myocardial tissue, and then HHA solution was dropped onto the ODS to form hydrogel on the surface of tissues. The hydrogel bonded to the myocardium could resist stretching, twisting, bending, and even water flushing without peeling off (Video S5). It is noted that after one side of ODS adhered to myocardial tissue, HHA was added to outer surface to form a hydrogel by consuming the remaining aldehydes. In this case, the top surface became nonsticky, avoiding adhesion to other tissues (Video S6). Clearly, the HHA@ODS that was gelled first and then attached to the myocardial tissue could not form firm adhesion since it was easily washed away by water flushing (Video S7). This verified that the ability of ODS to quickly remove interfacial water from the tissue surface was vital for wet adhesion. The firm adhesive performance of HHA@ODS hydrogel was also verified in vivo. As shown in Fig. 5G and Video S8, HHA@ODS hydrogel patch could firmly adhere to the surface of cardiac tissue of live rats, and maintain stable adhesion on beating heart surface even after 17 days. The cardiac patch was degraded completely after 28 days, evidencing its suitability for the treatment of MI (Fig. S13). Considering its outstanding wet tissue adhesion, we next determined the protective effect of HHA@ODS@HP-β-CD@Res on H9C2 cardiomyocytes under oxidative stress. We can find that HHA@ODS@HP-β-CD@Res enhanced the survival rate of H9C2 cardiomyocytes from 73% to 90% (Fig. S14). The protective effect of the HHA@ODS@HP-β-CD@Res hydrogel patch on MSCs under oxidative stress was also detected. As shown in Fig. S15, the death rate of MSCs in HHA@ODS hydrogel reached 19.7%, but it decreased to 5.7% in HHA@ODS@HP-β-CD@Res hydrogel, indicating that HHA@ODS@HP-β-CD@Res could significantly reduce the oxidative stress damage of MSCs. The paracrine effect of MSCs was determined by enzyme linked immunosorbent assay (ELISA). As presented in Fig. S16, MSCs could secrete proangiogenic, anti-inflammatory, and anti-apoptotic factors, which performed a significant function in cardiac repair after MI.

Supplementary data related to this article can be found at https://doi.org/10.1016/j.bioactmat.2022.07.029.

3.5. *Therapeutic effect of HHA@ODS@HP-β-CD@Res@MSCs adhesive hydrogel patch on MI of rats*

To further determine the repair effect of HHA@ODS@HP-β-CD@Res@MSCs on cardiac function after MI, rats were randomly divided into 6 groups (6 rats per group): Sham, MI, MI-HHA@ODS, MI-HHA@ODS@MSCs, MI-HHA@ODS@HP-β-CD@Res, and MI-HHA@ODS@HP-β-CD@Res@MSCs. Echocardiography data were collected at 28 days post-operation to assess cardiac function (Fig. 6A). The hearts were significantly deteriorated and severe infarction enlargement occurred after MI, but after treated with hydrogels, the cardiac function was improved. Especially, the HHA@ODS@HP-β-CD@Res@MSCs group demonstrated the best the therapeutic efficiencies with the highest EF and FS (EF: HHA@ODS@HP-β-CD@Res@MSCs: 73.70% ± 5.23% vs MI: 31.82% ± 7.18%; HHA@ODS hydrogel: 51.81% ± 8.26%; HHA@ODS@MSCs: 61.37% ± 2.61%; HHA@ODS@HP-β-CD@Res: 65.10% ± 3.52%) (FS: HHA@ODS@HP-β-CD@Res@MSCs: 43.52% ± 4.74% vs MI: 15.79% ± 3.91%; HHA@ODS: 27.48% ± 5.33%; HHA@ODS@MSCs: 33.72% ± 2.11%; HHA@ODS@HP-β-CD@Res: 36.89% ± 2.45%) (Fig. 6B and C). The results of Masson trichrome staining of heart tissues collected at 4 weeks showed that HHA@ODS@HP-β-CD@Res@MSCs group exhibited

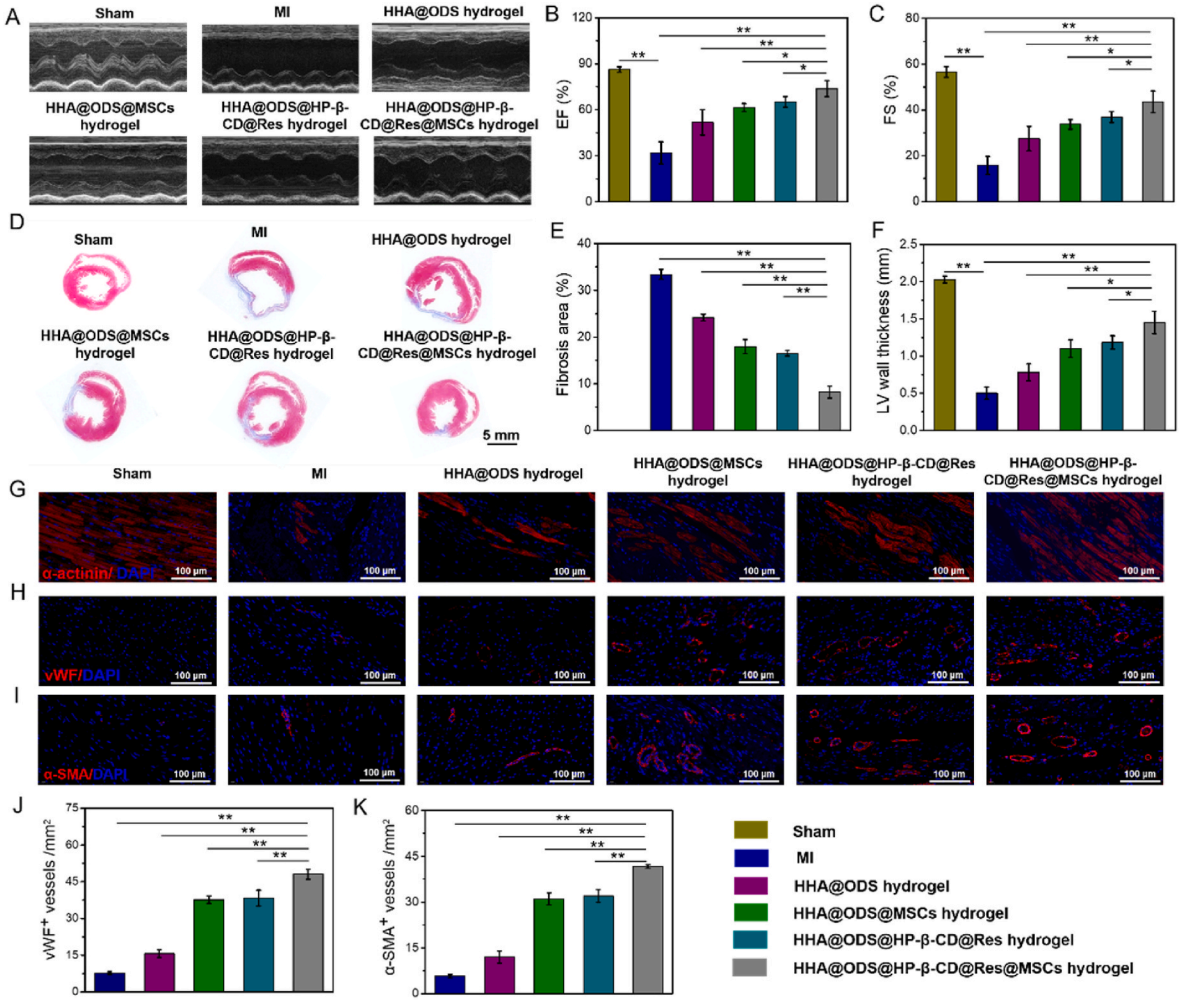

Fig. 6. Repair effect of different groups in MI rats. (A) Left-ventricular function determined with echocardiography 28 days after the transplantation in different groups. (B) Quantification analysis of cardiac function of EF and (C) FS. (D) Cardiac structures as indicated by the Masson trichrome staining. (E) Quantitative analysis of the fibrosis area and (F) LV wall thickness. (G) Representative immunofluorescent staining images of α-actintin, (H) vWF and (I) α-SMA at 28 days. (J) Quantification of the neovessels for vWF^+ vessels and (K) $\alpha\text{-SMA}^+$ vessels in the infarct regions after 28 days.

the smallest fibrosis area (HHA@ODS@HP-β-CD@Res@MSCs: 8.2% ± 1.25% vs MI: 33.40% ± 1.08%; HHA@ODS: 24.17% ± 0.71%; HHA@ODS@MSCs: 17.98% ± 1.51%; HHA@ODS@HP-β-CD@Res: 16.53% ± 0.55%) and the thickest LV wall (HHA@ODS@HP-β-CD@Res@MSCs: 1.45 mm ± 0.15 mm vs MI: 0.50 mm ± 0.08 mm; HHA@ODS hydrogel: 0.78 mm ± 0.11 mm; HHA@ODS@MSCs: 1.10 mm ± 0.12 mm; HHA@ODS@HP-β-CD@Res: 1.18 mm ± 0.09 mm) compared with other experimental groups (Fig. 6D–F). In addition, the MSCs were labeled by Cy7 DiC18 fluorescent reagent and the retention time was measured by in vivo imaging system (IVIS) on the 3, 14, and 21 days after operation (Fig. S17). Though the fluorescence gradually diminished over time, a small amount of fluorescence signal could still be detected at day 21 after transplantation, indicating that MSCs loaded into the cardiac patch could stay at MI heart in a sufficiently long time period for completing repair effect.

The cardiac structure in the infarcted area was determined by an immunofluorescence analysis. α-actinin, a key myocardial skeleton protein, whose expression is downregulated when the myocardium is damaged. As shown in Fig. 6G, only a small amount of α-actinin protein was detected in the MI group. In contrast, the expression of this protein increased in all cardiac patch treated groups, and the HHA@ODS@HP-β-CD@Res@MSCs group achieved the highest expression of α-actinin protein. Neovascularization including microvascular and small arterioles in the ischemic myocardium was also detected by vWF immunostaining and α-SMA immunostaining (Fig. 6H and I). In all treatment groups, HHA@ODS@HP-β-CD@Res@MSCs group resulted in the highest angiogenesis activity (Fig. 6J and K). Collectively, these results clearly demonstrated that adhesive hydrogel patch loading HP-β-CD@Res molecular capsules and MSCs could lead to highly efficient repair of cardiac function by promoting angiogenesis, and reducing cardiac fibrosis via concerted anti-oxidation and autophagy-regulating pathway.

4. Conclusion

In conclusion, we synthesized molecular capsules by loading anti-oxidant Res into the complexing agent HP-β-CD through host-guest interaction and studied their role in cardiac repair after MI. In vitro experiments demonstrated that HP-β-CD barely had the ROS-scavenging activity, but could protect H9C2 cardiomyocytes under oxidative stress by upregulating autophagy. Inclusion of Res endowed HP-β-CD@Res with the ability to scavenge ROS. The regulatory effect of HP-β-CD@Res on microenvironment after MI and promoting angiogenesis in infarcted area was verified in vivo. However, its improvement of cardiac function and cardiac structure were far from meeting the clinical needs due to the rapid clean-up of HP-β-CD and HP-β-CD@Res from the body. We demonstrated that HP-β-CD@Res-loaded aldehyde-modified dextran sponge (ODS) could be firmly adhered to the surface of wet myocardium

as a fixed carpet via quick capillary removing interfacial water from the tissue surface and Schiff base reaction. An aqueous biocompatible hydrazided hyaluronic acid (HHA) solution mixed with MSCs was impregnated into the fixed sponge carpet to form HHA@ODS@HP-β-CD@Res@MSCs hydrogel in situ via click reaction, thus prolonging the in vivo retention time of HP-β-CD@Res and MSCs. After inner side of ODS bonded to myocardial tissue, the remaining aldehyde groups on the outer surface were consumed by the added HHA, resulting in a nonsticky top surface, which could prevent adhesion to other tissues. The embedded HP-β-CD@Res molecular capsules in the fixed hydrogel carpet could improve cardiac microenvironment, reduce cardiomyocyte apoptosis, and enhance the survival of transplanted stem cells by scavenging ROS and upregulating autophagy, and the transplanted stem cells could also secrete proangiogenic, anti-inflammatory, and anti-apoptotic factors, thus facilitating angiogenesis and reducing cardiac fibrosis to efficiently repair infarcted myocardium. This wet adhesive hydrogel patch loaded with anti-oxidative, autophagy-regulating molecule capsules can expanded to repair and regeneration of different soft tissues. In addition, several strategies need to be employed to further improve the wet adhesive strength of HHA@ODS hydrogels to wet tissues: one is to improve the interface drainage capacity, the other is to increase the content of surface adhesion groups, the third is to balance the interface energy and cohesion energy.

CRediT authorship contribution statement

Tengling Wu: Investigation, Data curation, Methodology, Formal analysis, Writing – original draft. **Xiaoping Zhang:** Investigation, Data curation. **Yang Liu:** Software, Data curation. **Chunyan Cui:** Investigation, Data curation. **Yage Sun:** Software, Data curation. **Wenguang Liu:** Conceptualization, Formal analysis, Writing – review & editing.

Declaration of competing interest

The authors declare no conflicts of interest.

Acknowledgements

The authors gratefully acknowledge the support for this work from the National Natural Science Foundation of China (Grant No. 52233008, 51733006), and the National Key Research and Development Program (Grant No. 2018YFA0703100).

Appendix A. Supplementary data

Supplementary data to this article can be found online at https://doi.org/10.1016/j.bioactmat.2022.07.029.

References

[1] X.P. Zhang, W.G. Liu, Engineering injectable anti-inflammatory hydrogels to treat acute myocardial infarction, Adv. NanoBiomed Res. (2022), 2200008.
[2] S. Sahoo, D.W. Losordo, Exosomes and cardiac repair after myocardial infarction, Circ. Res. 114 (2014) 333–344.
[3] H. Hashimoto, E.N. Olson, R. Bassel-Duby, Therapeutic approaches for cardiac regeneration and repair, Nat. Rev. Cardiol. 15 (2018) 585–600.
[4] T.L. Wu, W.G. Liu, Functional hydrogels for the treatment of myocardial infarction, NPG Asia Mater. 14 (2022) 9.
[5] E. Marban, A mechanistic roadmap for the clinical application of cardiac cell therapies, Nat. Biomed. Eng. 2 (2018) 353–361.
[6] V. Sampaio-Pinto, J. Janssen, N. Chirico, M. Serra, P.M. Alves, P.A. Doevendans, I. K. Voets, J.P.G. Sluijter, L.W. van Laake, A. van Mil, A roadmap to cardiac tissue-engineered construct preservation: insights from cells, tissues, and organs, Adv. Mater. 33 (2021), 2008517.
[7] T.L. Wu, C.Y. Cui, Y.T. Huang, Y. Liu, C.C. Fan, X.X. Han, Y. Yang, Z.Y. Xu, B. Liu, G.W. Fan, W.G. Liu, Coadministration of an adhesive conductive hydrogel patch and an injectable hydrogel to treat myocardial infarction, ACS Appl. Mater. Interfaces 12 (2020) 2039–2048.
[8] S. Pedron, S. van Lierop, P. Horstman, R. Penterman, D.J. Broer, E. Peeters, Stimuli Responsive delivery vehicles for cardiac microtissue transplantation, Adv. Funct. Mater. 21 (2011) 1624–1630.
[9] G. Choe, S.W. Kim, J. Park, J. Park, S. Kim, Y.S. Kim, Y. Ahn, D.W. Jung, D. R. Williams, J.Y. Lee, Anti-oxidant activity reinforced reduced graphene oxide/alginate microgels: mesenchymal stem cell encapsulation and regeneration of infarcted hearts, Biomaterials 225 (2019), 119513.
[10] A. Singh, A. Singh, D. Sen, Mesenchymal stem cells in cardiac regeneration: a detailed progress report of the last 6 years (2010-2015), Stem Cell Res. Ther. 7 (2016) 82.
[11] Y. Liu, X.P. Zhang, T.L. Wu, B. Liu, J.H. Yang, W.G. Liu, Chinese herb-crosslinked hydrogel bearing rBMSCs-laden polyzwitterion microgels: self-adaptive manipulation of micromilieu and stemness maintenance for restoring infarcted myocardium, Nano Today 41 (2021), 101306.
[12] T. Hao, J.J. Li, F.L. Yao, D.Y. Dong, Y. Wang, B.G. Yang, C.Y. Wang, Injectable fullerenol/alginate hydrogel for suppression of oxidative stress damage in brown adipose-derived stem cells and cardiac repair, ACS Nano 11 (2017) 5474–5488.
[13] Y. Sun, Myocardial repair/remodeling following infarction: roles of local factors, Cardiovasc. Res. 81 (2009) 482–490.
[14] K.A. Spaulding, Y. Zhu, K. Takaba, A. Ramasubramanian, A. Badathala, H. Haraldsson, A. Collins, E. Aguayo, C. Shah, A.W. Wallace, N.P. Ziats, D. H. Lovett, A.J. Baker, K.E. Healy, M.B. Ratcliffe, Myocardial injection of a thermoresponsive hydrogel with reactive oxygen species scavenger properties improves border zone contractility, J. Biomed. Mater. Res. 108 (2020) 1736–1746.
[15] Y.H. Cheng, F.H. Lin, C.Y. Wang, C.Y. Hsiao, H.C. Chen, H.Y. Kuo, T.F. Tsai, S. H. Chiou, Recovery of oxidative stress-induced damage in Cisd2-deficient cardiomyocytes by sustained release of ferulic acid from injectable hydrogel, Biomaterials 103 (2016) 207–218.
[16] W. Wang, J.R. Chen, M. Li, H.Z. Jia, X.X. Han, J.X. Zhang, Y. Zou, B.Y. Tan, W. Liang, Y.Y. Shang, Q. Xu, S. A, W.X. Wang, J.Y. Mao, X.M. Gao, G.W. Fan, W. G. Liu, Rebuilding post-infarcted cardiac functions by injecting TIIA@PDA NPs-crosslinked ROS sensitive hydrogels, ACS Appl. Mater. Interfaces 11 (2019) 2880–2890.
[17] J. Ding, Y.J. Yao, J.W. Li, Y.Y. Duan, J.R. Nakkala, X. Feng, W.B. Cao, Y.C. Wang, L. J. Hong, L.Y. Shen, Z.W. Mao, Y. Zhu, C.Y. Gao, A reactive oxygen species scavenging and O_2 generating injectable hydrogel for myocardial infarction treatment in vivo, Small 16 (2020), 2005038.
[18] Y. Zhu, Y. Matsumura, M. Velayutham, L.M. Foley, T.K. Hitchens, W.R. Wagner, Reactive oxygen species scavenging with a biodegradable, thermally responsive hydrogel compatible with soft tissue injection, Biomaterials 177 (2018) 98–112.
[19] X.X. Han, L. Li, T. Xie, S. Chen, Y. Zou, X. Jin, S. Li, M. Wang, N. Han, G.W. Fan, W. G. Liu, W. Wang, Ferrero-like" nanoparticles knotted injectable hydrogels to initially scavenge ROS and lastingly promote vascularization in infarcted hearts, Sci. China Technol. Sci. 63 (2020) 2435–2448.
[20] X.Q. Wu, Z.M. Liu, X.Y. Yu, S.W. Xu, J.D. Luo, Autophagy and cardiac diseases: therapeutic potential of natural products, Med. Res. Rev. 41 (2021) 314–341.
[21] H.H. Liang, X.M. Su, Q.X. Wu, H.T. Shan, L.F. Lv, T. Yu, X.G. Zhao, J. Sun, R. Yang, L. Zhang, H. Yan, Y.H. Zhou, X.L. Li, Z.M. Du, H.L. Shan, LncRNA 2810403D21Rik/Mirf promotes ischemic myocardial injury by regulating autophagy through targeting Mir26a, Autophagy 16 (2020) 1077–1091.
[22] H. Liu, S.Y. Liu, X.Y. Qiu, X.S. Yang, L.L. Bao, F.X. Pu, X.M. Liu, C.Y. Li, K. Xuan, J. Zhou, Z.H. Deng, S.Y. Liu, Y. Jin, Donor MSCs release apoptotic bodies to improve myocardial infarction via autophagy regulation in recipient cells, Autophagy 16 (2020) 2140–2155.
[23] X.Q. Wu, L.S. He, F.J. Chen, X.E. He, Y. Cai, G.P. Zhang, Q. Yi, M.X. He, J.D. Luo, Impaired autophagy contributes to adverse cardiac remodeling in acute myocardial infarction, PLoS One 9 (2014), e112891.
[24] M. Yokoo, Y. Kubota, K. Motoyama, T. Higashi, M. Taniyoshi, H. Tokumaru, R. Nishiyama, Y. Tabe, S. Mochinaga, A. Sato, N. Sueoka-Aragane, E. Sueoka, H. Arima, T. Irie, S. Kimura, 2-Hydroxypropyl-β-cyclodextrin acts as a novel anticancer agent, PLoS One 10 (2015), e0141946.
[25] S. Dai, A.E. Dulcey, X. Hu, C.A. Wassif, F.D. Porter, C.P. Austin, D.S. Ory, J. Marugan, W. Zheng, Methyl-β-cyclodextrin restores impaired autophagy flux in Niemann-Pick C1-deficient cells through activation of AMPK, Autophagy 13 (2017) 1435–1451.
[26] K. Kilpatrick, Y.M. Zeng, T. Hancock, L. Segatori, Genetic and chemical activation of TFEB mediates clearance of aggregated α-synuclein, PLoS One 10 (2015), e0120819.
[27] S. Zimmer, A. Grebe, S.S. Bakke, N. Bode, B. Halvorsen, T. Ulas, M. Skjelland, D. D. Nardo, L.I. Labzin, A. Kerksiek, C. Hempel, M.T. Heneka, V. Hawxhurst, M. L. Fitzgerald, J. Trebicka, I. Björkhem, J. Gustafsson, M. Westerterp, A.R. Tall, S. D. Wright, T. Espevik, J.L. Schultze, G. Nickenig, D. Lütjohann, E. Latz, Cyclodextrin promotes atherosclerosis regression via macrophage reprogramming, Sci. Transl. Med. 8 (2016) 333.
[28] N. Summerlin, Z. Qu, N. Pujara, Y. Sheng, S. Jambhrunkar, M. McGuckin, A. Popat, Colloidal mesoporous silica nanoparticles enhance the biological activity of resveratrol, Colloids Surf., B 144 (2016) 1–7.
[29] S. Kaga, L.J. Zhan, M. Matsumoto, N. Maulik, Resveratrol enhances neovascularization in the infarcted rat myocardium through the induction of thioredoxin-1, heme oxygenase-1 and vascular endothelial growth factor, J. Mol. Cell. Cardiol. 39 (2005) 813–822.
[30] H. Lee, B.P. Lee, P.B. Messersmith, A reversible wet/dry adhesive inspired by mussels and geckos, Nature 448 (2007) 338–341.
[31] C.Y. Cui, W.G. Liu, Recent advances in wet adhesives: adhesion mechanism, design principle and applications, Prog. Polym. Sci. 116 (2021), 101388.
[32] H. Yuk, C.E. Varela, C.S. Nabzdyk, X.Y. Mao, R.F. Padera, E.T. Roche, X.H. Zhao, Dry double-sided tape for adhesion of wet tissues and devices, Nature 575 (2019) 169–174.

[33] J. Shin, S. Choi, J.H. Kim, J.H. Cho, Y. Jin, S. Kim, S. Min, S.K. Kim, D. Choi, S. W. Cho, Tissue tapes-phenolic hyaluronic acid hydrogel patches for off-the-shelf therapy, Adv. Funct. Mater. 29 (2019), 1903863.
[34] X. Peng, X.F. Xia, X.Y. Xu, X.F. Yang, B.G. Yang, P.C. Zhao, W.H. Yuan, P.W. Y. Chiu, L.M. Bian, Ultrafast self-gelling powder mediates robust wet adhesion to promote healing of gastrointestinal perforations, Sci. Adv. 7 (2021), eabe8739.
[35] K. Kaur, S. Uppal, R. Kaur, J. Agarwal, S.K. Mehta, Energy efficient, facile and cost effective methodology for formation of an inclusion complex of resveratrol with hp-β-CD, New J. Chem. 39 (2015) 8855–8865.
[36] N. Rajendiran, S. Siva, Inclusion complex of sulfadimethoxine with cyclodextrins: preparation and characterization, Carbohydr. Polym. 101 (2014) 828–836.
[37] Z.J. Luo, Y.H. Min, L.L. Qu, Y.Y. Song, Y.X. Hong, Remediation of phenanthrene contaminated soil by ferrous oxalate and its phytotoxicity evaluation, Chemosphere 265 (2021), 129070.
[38] X.Q. Wu, D.C. Zheng, Y.Y. Qin, Z.M. Liu, G.P. Zhang, X.Y. Zhu, L.H. Zeng, Z. Y. Liang, Nobiletin attenuates adverse cardiac remodeling after acute myocardial infarction in rats via restoring autophagy flux, Biochem. Bioph. Res. Co. 492 (2017) 262e268.
[39] H. Kanamori, G. Takemura, K. Goto, A. Tsujimoto, A. Ogino, T. Takeyama, T. Kawaguchi, T. Watanabe, K. Morishita, M. Kawasaki, A. Mikami, T. Fujiwara, H. Fujiwara, M. Seishima, S. Minatoguchi, Resveratrol reverses remodeling in hearts with large, old myocardial infarctions through enhanced autophagy-activating AMP kinase pathway, Am. J. Pathol. 182 (2013) 701–713.
[40] Q. Jiang, J. Yin, J.S. Chen, X.K. Ma, M.M. Wu, G. Liu, K. Yao, B. Tan, Y.L. Yin, Mitochondria-targeted antioxidants: a step towards disease treatment, Oxid. Med. Cell. Longev. 20 (2020) 1–18.
[41] X. Qi, Y.H. Yuan, K. Xu, H.S. Zhong, Z. Zhang, H. Zhai, G.F. Guan, G.B. Yu, (2-Hydroxypropyl)-β-cyclodextrin is a new angiogenic molecule for therapeutic angiogenesis, PLoS One 10 (2015), e0125323.
[42] S. Liang, Y.Y. Zhang, H.B. Wang, Z.Y. Xu, J.R. Chen, R. Bao, B.Y. Tan, Y.L. Cui, G. W. Fan, W.X. Wang, W. Wang, W.G. Liu, Paintable and rapidly bondable conductive hydrogels as therapeutic cardiac patches, Adv. Mater. 30 (2018), 1704235.
[43] Y. Zhang, A. Khalique, X.C. Du, Z.X. Gao, J. Wu, X.Y. Zhang, R. Zhang, Z.Y. Sun, Q. Q. Liu, Z.L. Xu, A.C. Midgley, L.Y. Wang, X.Y. Yan, J. Zhuang, D.L. Kong, X. L. Huang, Biomimetic design of mitochondria-targeted hybrid nanozymes as superoxide scavengers, Adv. Mater. 33 (2021), 2006570.
[44] C.Y. Liu, X. Liu, C.Y. Liu, N. Wang, H.L. Chen, W.H. Yao, G.Z. Sun, Q.L. Song, W. H. Qiao, A highly efficient, in situ wet-adhesive dextran derivative sponge for rapid hemostasis, Biomaterials 205 (2019) 23–37.
[45] X.P. Zhang, Y.N. Lyu, Y. Liu, R. Yang, B. Liu, J. Li, Z.Y. Xu, Q. Zhang, J.H. Yang, W. G. Liu, Artificial apoptotic cells/VEGF-loaded injectable hydrogel united with immunomodification and revascularization functions to reduce cardiac remodeling after myocardial infarction, Nano Today 39 (2021), 101227.